JOURNAL OF MATERIALS SCIENCE 30 (1995) 2330–2337

Correlation of geometry effects with fracture toughness by damage equivalence

FASHANG MA*
Department of Engineering Mechanics, Xian Jiaotong University, Xian 710049, People's Republic of China

The near crack tip porosity fields in different fracture specimens, single edge notched, single edge notched loaded in centre of ligament, three point bending specimens, and small scale yielding (SSY) mode have been studied by the finite deformation finite element method. The presence and subsequent growth of smaller-scale voids were taken into account by using Gurson's model to describe the constitutive behaviour of the material. Based on damage equivalence at a characteristic position in the SSY mode and actual fracture specimens, the ratio of scaling parameters, J values, in both modes was obtained, and was used to eliminate the geometry dependence of fracture toughness through correlations to the small scale yielding mode.

1. Introduction

For large scale yielding problems in finite bodies, the relationship between the scaling parameter, J (Rice's J integral [1]), and the near crack tip fields loses the one-to-one correspondence [2–4]; this loss of uniqueness, termed loss of constraint, produces increases in fracture toughness observed for tension geometries and for shallow notch bend specimens. The mismatch of constraint conditions in the tip region apparently plays a dominant role in the often disappointing correlation between different specimen behaviours and the behaviour observed in small scale yielding. To address the near tip constraint, Al-Ani and Hancock [2] and Betegon and Hancock [5] correlated the loss of J dominance with the second term, T stress, in the asymptotic expansion of the elastic field. The detailed elastic–plastic finite element analysis of O' Dowd and Shih [3, 4] provided correlations of crack tip stress fields over distances of $2 - 8\delta_t$, where δ_t is the crack tip opening displacement with loading level, J, loading model (tension versus bending), specimen geometry and strain hardening. Their computations stimulated development of a scaling-hydrostatic stress, J–Q continuum mechanics framework [6, 7] to describe the near tip fields under very general conditions of loading in finite bodies. The Q, hydrostatic stress parameter, termed Q stress, quantifies the level of stress triaxiality in the tip region.

Various mechanisms compete to be the controlling mode of fracture in metals [8–13]. In most steels, for instance, the controlling mechanism of fracture at sufficiently low temperatures is brittle cleavage, accompanied by a little plastic deformation, while at relatively high temperatures the mechanism is primarily nucleation, growth and coalescence of microvoids ahead of the crack tip [14, 15]; or, both mechanisms may be active. Mechanisms of correlating cleavage mode to macroscopic fracture toughness were conducted by [16, 17] for a mild steel. The effects of constraint on cleavage mode were determined by stress fields calculated from finite element analysis [18, 19] and J–Q descriptions [6] of crack tip fields. But for ductile fracture, where the dominant mechanism is void coalescence, the effects of constraint on stress, deformation, porosity and macroscopic fracture toughness still remain open.

Ductile fracture by void mechanisms has long been observed in metals. The fracture process begins with the nucleation of voids at inclusions, precipitates, or any other weak interface, and this is followed by growth of these voids and ultimate fracture of the specimen by coalescence of neighbouring voids or the void and crack. Rice and Johnson [20] calculated the critical crack tip opening displacement of a plane strain tensile crack, as a function of inclusion size and spacing, using a slip line field analysis that accounts for finite geometry change, in conjunction with the results of Rice and Tracey [21], for the growth of an isolated spherical void. Final coalescence of the void with the crack is assumed to occur when the width of the ligament between the crack and the void is equal to the maximum dimension of the void. The coupling of progressive fracture events with the surrounding deformation field was addressed by [22–24] through large deformation finite element analyses of the interaction between a single cylindrical void and a plane strain tensile crack. Aravas and McMeeking [24] used standard J_2 flow theory in a fully dense material, while Aoki *et al.* [22] and Aravas and McMeeking [23] employed Gurson's model [25] to represent the small

* On leave, Department of Mechanical and Intelligent Systems Engineering, Tokyo Institute of Technology, Tokyo, Japan.

0022–2461

scale voids as suggested by [26]; Aravas and McMeeking [23] also applied the modification of Tvergaard and Needleman [27] to predict the coalescence of voids at a realistic void volume fraction. Needleman and Tvergaard [28] examined different scale void distributions and analysed the microscopic fracture mechanism in detail to predict macroscopic toughness. Jagota *et al.* [17] employed Gurson's model to study stress and porosity fields near a crack tip, and predicted fracture toughness for mode I crack in a porous elastic–plastic solid. In each of these studies, the small scale yielding (SSY) condition was used, i.e. the displacements of linear elastic fracture mechanics (K field) were used as conditions to determine the local stresses, deformations and porosities. Recently, Ma and Kuang [29] analysed stresses, deformations and porosities in standard fracture specimens, and found that the loss of constraint plays an important role in the increase of fracture toughness for tension geometries.

The present work focuses on quantifying specimen geometry effects for initiation of crack growth in ductile materials. The near crack tip porosity fields in different fracture specimens, single edge notched (SEN1), single edge nothced (SEN2) loaded in centre of ligament, three point bending (TPB) specimens, which were used in the experiment of Hancock and Cowling [30] and SSY mode have been studied by the finite deformation finite element method. The presence and subsequent growth of smaller scale voids were taken into account by using Gurson's model to describe the constitutive behaviour of the material. A microscopic, void coalescence criterion for initiation of crack growth in ductile materials will be adopted to relate the macroscopic fracture parameters in different actual fracture specimens and SSY mode, which impose identical damage values at a characteristic position ahead of a blunting crack; and the geometry dependence of fracture toughness data for different specimens will be eliminated through correlations to the SSY mode.

2. Discussion

2.1. Constitutive relations

In order to describe the complete loss of material stress carrying capacity at ductile fracture due to the coalescence of voids at a realistic level of the void volume fraction, Tvergaard and Needleman [27] modified Gurson's porous plastic model as follows

$$\phi = \frac{\sigma_e^2}{\sigma_M^2} + 2f^* q_1 \cosh\left(\frac{q_2 \sigma_{kk}}{2\sigma_M}\right) - [1 + (q_1 f^*)^2] = 0 \quad (1)$$

where σ_e is the macroscopic equivalent stress, σ_M is an equivalent tensile flow stress representing the actual microscopic stress state in the matrix material, q_1 and q_2 were introduced by Tvergaard [26] in an attempt to make the predictions of Gurson's model agree with numerical studies of materials containing periodically distributed circular cylindrical voids, f^* is defined in [27] as

$$f^* = \begin{cases} f & \text{for } f \leqslant f_c \\ f_c + k(f - f_e) & \text{for } f > f_c \end{cases} \quad (2)$$

$$k = \frac{f_u^* - f_c}{f_F - f_c} \quad (3)$$

where f represents the current void volume fraction, and is a measure of damage of material; f_c was proposed to limit the direct application of Gurson's model, and f_F denotes the void volume fraction at final fracture. Setting $\sigma_{ij} = 0$ in Equation 1, it is found that the macroscopic stress carrying capacity vanishes for

$$f^* = f_u^* = f^*(f_F) = 1/q_1 \quad (4)$$

It is assumed that the microscopic equivalent plastic strain ε_M in the matrix material is determined by the principle of equivalent plastic work

$$\sigma_{ij} D_{ij}^p = (1 - f)\sigma_M \dot{\varepsilon}_M^p \quad (5)$$

where the superposed dot denotes the material time derivative, D_{ij}^p is the plastic part of the deformation rate tensor, D_{ij}.

$$D_{ij} = \tfrac{1}{2}(v_{i,j} + v_{j,i}) \quad (6)$$

where v_i is the velocity component and x_i the current position component of a material point in Cartesian co-ordinates. The relation between σ_M and ε_M^p is

$$h_M = \frac{d\sigma_M}{d\varepsilon_M^p} \quad (7)$$

thus

$$\dot{\sigma}_M = h_M \frac{\sigma_{ij} D_{ij}^p}{(1 - f)\sigma_M} \quad (8)$$

The changes in the void volume fraction result from void nucleation, $\dot{f}_N$, as well as from the growth of existing voids

$$\dot{f} = \dot{f}_{growth} + \dot{f}_N \quad (9)$$

The growth of existing voids with deformation is determined from the condition for plastic incompressibility of the matrix material

$$\dot{f}_{growth} = (1 - f) D_{kk}^p \quad (10)$$

The contribution resulting from the nucleation of new voids is taken to be

$$\dot{f}_N = B(\dot{\sigma}_M + \dot{\sigma}_m) + A\dot{\varepsilon}_M^p \quad (11)$$

Void nucleation is taken to follow a normal distribution [31], so that stress controlled nucleation is specified by

$$B = \frac{f_N}{\sigma_0 S_N (2\pi)^{1/2}} \exp\left[-\frac{1}{2}\left(\frac{\sigma_M + \sigma_m - \sigma_N}{\sigma_Y S_N}\right)^2 \right]; \quad A = 0 \quad (12)$$

where f_N is the volume fraction of void nucleating particles, σ_N is the mean critical stress for nucleation, and S_N is the standard deviation of the normal distribution.

For plastic strain controlled nucleation with mean nucleation strain, ε_N, analogous expressions are

$$A = \frac{f_N}{S_N(2\pi)^{1/2}}\exp\left[-\frac{1}{2}\left(\frac{\varepsilon_M^p - \varepsilon_N}{S_N}\right)^2\right]; \quad B = 0 \tag{13}$$

The plastic strain controlled nucleation was used in the remainder of this paper.

Similar to classical plasticity [32], the plastic flow rule is

$$D_{ij}^p = \lambda\frac{\partial\phi}{\partial\sigma_{ij}} \tag{14}$$

where λ is the plastic flow factor determined from the consistency condition

$$\dot{\phi} = 0 \tag{15}$$

during plastic loading.

Substituting Equations 8–11 into Equation 15, and solving for λ the constitutive equations for porous plasticity are finally found

$$\sigma_{ij}^J = \frac{E}{1+v}D_{ij} + \frac{E}{1-2v}\delta_{ij}D_{kk} - \frac{E}{1-2v}\frac{N_{ij}N_{kl}D_{kl}}{C}$$

$$C = (1-2v)\left(\frac{H}{E}\right) + \frac{3(1-2v)}{2(1+v)}\omega + 3\alpha^2$$

$$N_{ij} = \frac{3(1-2v)}{2(1+v)}\frac{\sigma_{ij}}{\sigma_M} + \alpha\delta_{ij} \tag{16}$$

and

$$H = \frac{h_M}{1-f}\left(\omega + \alpha\frac{\sigma_{kk}}{\sigma_M}\right)\left(\omega + \alpha\frac{\sigma_{kk}}{\sigma_M} - \sigma_M A\gamma\frac{\partial f^*}{\partial f}\right) - 3\sigma_M(1-f)\alpha\gamma\frac{\partial f^*}{\partial f}$$

$$\alpha = \frac{1}{2}q\times f^*\sinh\left(\frac{\sigma_{kk}}{2\sigma_M}\right)$$

$$\gamma = \frac{1}{2}\frac{\partial\phi}{\partial f^*} = q_1\cosh\left(\frac{\sigma_{kk}}{2\sigma_M}\right) - q_1^2 f^*$$

$$\omega = 1 + (q_1 f^*)^2 - 2q_1 f^*\cosh\left(\frac{\sigma_{kk}}{2\sigma_M}\right)$$

where

$$\sigma_{ij}^J = \dot{\sigma}_{ij} - \Omega_{ip}\sigma_{pj} - \sigma_{ik}\Omega_{jk} \tag{17}$$

is the Jaumann objective rate of Euler stress tensor, and Ω is material element spin,

$$\Omega_{ij} = \tfrac{1}{2}(v_{i,j} - v_{j,i})$$

2.2. Finite element solutions

The updated Lagrangian scheme is used here, the variational equation in the rate form [33] is

$$\int_V\left[\sigma_{ij}^J\delta D_{ij} - \frac{1}{2}\sigma_{ij}\delta(2D_{ik}D_{kj} - v_{k,j}v_{k,i})\right]dv + \int_V\sigma_{ij}v_{k,k}\delta D_{ij}dv = \int_V\dot{F}_i\delta v_i dv + \int_{S_T}\dot{T}_i\delta v_i dx \tag{18}$$

where V is the volume of any part of the body, S_T is surface where the traction vector, T_i was prescribed; F_i the body force per unit volume, δv_i is an arbitrary virtual velocity variation which vanishes where the velocity is prescribed. The finite element analysis was based on the variational principle, Equation 18, and was done incrementally with equilibrium correction at the end of each increment.

The incremental J integral in large scale deformation problems is of the form [34]

$$\Delta J = \int_\Gamma(t_{ij}\Delta u_{i,j}n_1 - t_{ij}n_j\Delta u_{j,1} - \Delta t_{ij}n_j u_{i,1})ds \tag{19}$$

where t_{ij} is the Lagrange stress tensor and equals the Euler stress tensor, σ_{ij}, at the beginning of an increment step, N, but t_{ij} is not equal to σ_{ij} at the end of this step; Γ is a curve surrounding the crack tip, and the integral is evaluated in a contraclockwise sense starting from the lower flat crack surface and continuing along the path to the upper flat surface.

The specimen geometries and sizes of SEN1, SEN2 and TPB are shown in Fig. 1, and the ratios of crack depth, a, to specimen width, w, in three of the specimens are equal to 0.5. Eight node isoparametric elements are used. The local fine finite element mesh, as shown in Fig. 2, is surrounded by that shown in Fig. 3, the crack tip is modelled as a blunt notch with a radius r_0 of 5 μm. Due to symmetry, half of the specimens are simulated by the meshes in Figs 2 and 3. The mesh dependence of stress was investigated by Ma and Kuang [29]; they found that in the case of no tendency for localization of plastic flow, as observed by Aravas and McMeeking [23], the finite element mesh in Fig. 2 is appropriate to obtain stress, deformation and porosity in the vicinity of a blunting crack.

For the SSY model, the displacement boundary conditions imposed at the outer semicircular boundary are of the form

$$u_x = \frac{K_I}{E}(1+v)\frac{r_b}{2\pi}(3-4v-\cos\theta)\cos\frac{\theta}{2}$$

$$u_y = \frac{K_I}{E}(1+v)\frac{r_b}{2\pi}(3-4v-\cos\theta)\sin\frac{\theta}{2} \tag{20}$$

where u_x and u_y are Cartesian components of the displacement vector, r and θ are polar co-ordinates concentric with the semicircular notch centre. r_b is the value of r at the outer boundary, K_I is the mode I stress intensity factor and v is Poisson's ratio, E is Young's modulus. In this paper the outer radius of the outer perimeter, r_b is 2000 times the initial notch radius r_0. The near tip fine finite element mesh is shown in Fig. 2.

The hardening rule of the matrix material in uniaxial tensile testing in Gurson's model is specified by

$$\sigma_M = \sigma_0 + K(\varepsilon_M^p)^n \tag{21}$$

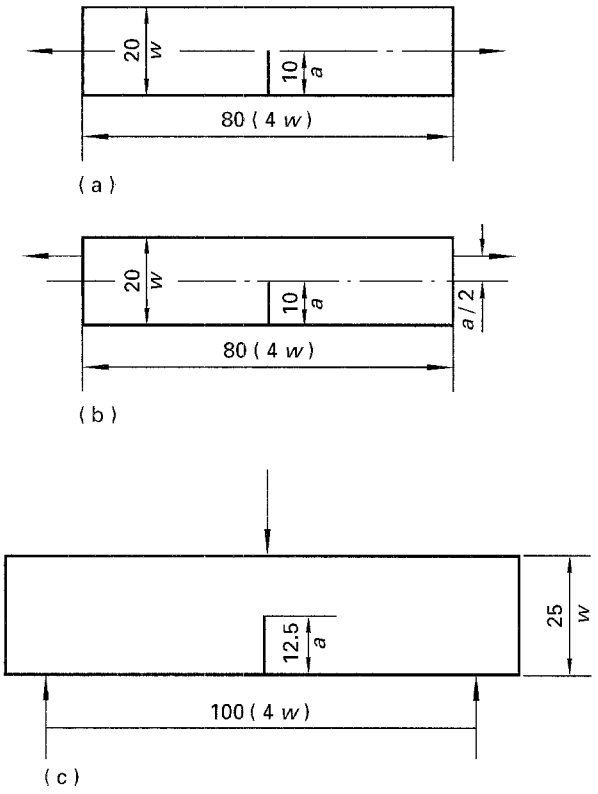

Figure 1 The gometries and sizes of (a) single edge notch (SEN1), (b) single edge notched loaded in centre of ligament (SEN2) and (c) three point bending (TPB) specimens.

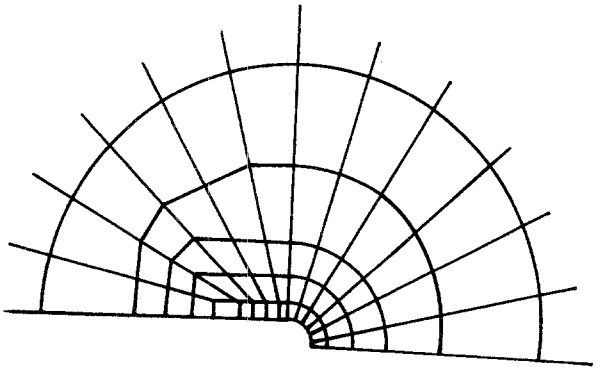

Figure 2 The local fine finite element mesh for its SSY mode, SEN1, SEN2 and TPB specimens

where σ_M and σ_0 are the flow stress and initial yield stress of matrix material, respectively, K and n are the hardening parameters. Following Aravas and McMeeking [23], the material parameters in Equation 1 are taken to be $q_1 = 1.25$, $f_c = 0.15$, $f_F = 0.25$, $\varepsilon_N = 0.3$, $S_N = 0.1$, $f_N = 0.04$, the initial void volume fraction is taken to be zero.

When the condition $f_u^* = 1/q_1$ (or equivalently $f = f_F$) is met at a material point, no more macroscopic stress can be carried and local failure occurs at that point. The method proposed by Tvergaard [35], and used by Avaras and McMeeking [23], is used here to model the material failure process. The constitutive law described earlier is used until the void volume fraction, f,equals $0.95 f_F$. Subsequently, the failed material is modelled by the elastic–plastic constitutive

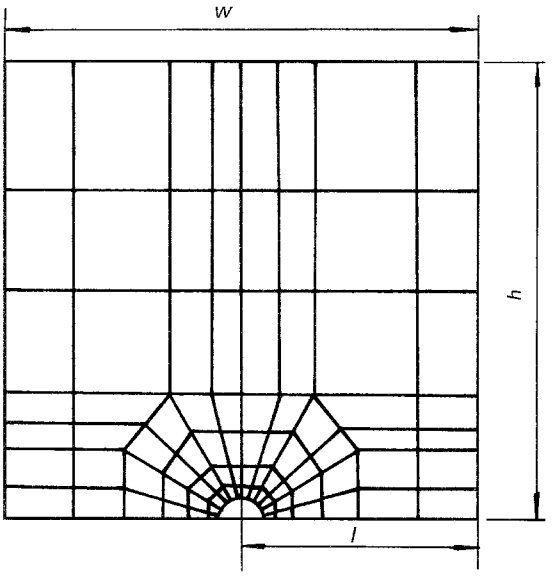

Figure 3 The finite element mesh surrounding that shown in Fig. 2 for SEN1, SEN2 and TPB specimens: (w) width, (h) height, (l) length.

equations described in Section 2.1, but with a constant volume fraction, f, equal to $0.95 f_F$. Also, at this stage, the microscopic yield stress is kept constant. In this way, the macroscopic stress state is forced to stay on a stress–strain curve corresponding to f equal to $0.95 f_F$, which is obtained by integrating Equation 16 for an axisymmetric tension with a superposed hydrostatic stress [23]. The condition $f = 0.95 f_F$ is used here also instead of $f = f_F$ due to the numerical problems.

2.3. Near crack tip porosities and deformations

The material considered here is HY80 steel used in Hancock and Cowling [30]; the material parameters are: $\sigma_0 = 560$ MPa, $n = 0.1$, $K = 1070$ MPa, Young's modulus $E = 210$ GPa and Poisson's ratio, $\nu = 0.3$.

2.3.1. Crack tip porosities

The variation of porosity, f, with r ahead of the blunting crack tip is shown in Fig. 4a–c for SEN1, SEN2 and TPB specimens; for comparison, the result for the SSY model is also depicted in the figures, the distance r is normalized by J/σ_0. The porosity reaches higher values, $f = 0.95 f_F$, close to the crack tip, the stress in the region is practically zero, i.e. complete loss of the stress carrying capacity in this region occurs. It is clear that the loss in the SSY model is larger than that in the other three specimens, the damaged zone (in which $f = 0.95 f_F$ is satisfied) in the SSY model is larger than that in the three other specimens. This may be the reason that the finite element result in the SSY model underestimates the critical crack tip opening displacement at fracture initiation.

As known, material damage results from plastic deformation and triaxiality. At lower load levels, the

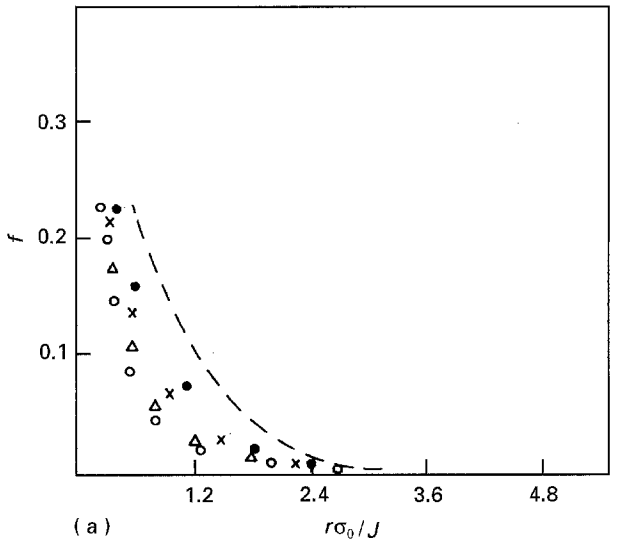

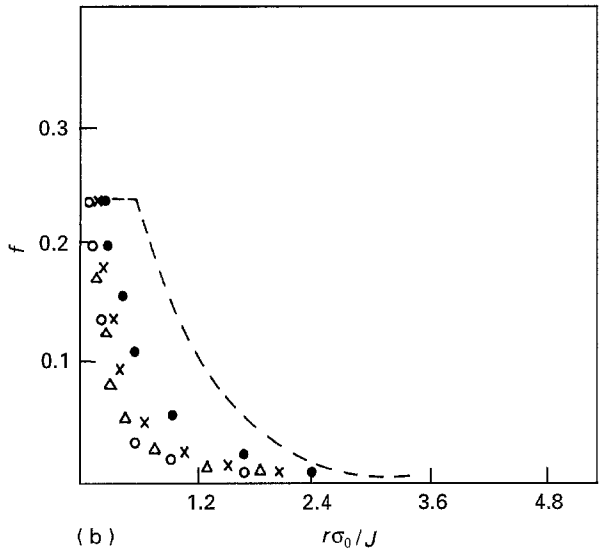

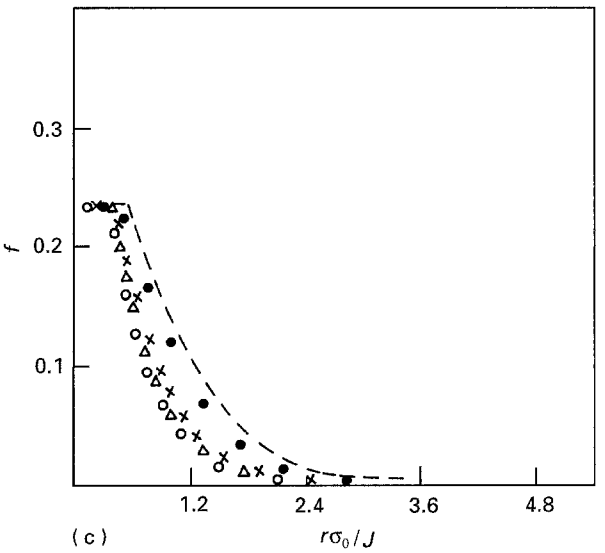

Figure 4 Porosity (f) in the uncracked ligament as a function of distance, r, from the current blunting crack centre at different loads in (a) SEN1 specimen and SSY mode, (b) SEN2 specimen and SSY mode, and (c) TPB and SSY mode. For $L\sigma_0/J$ equal to: (—) SSY, (●) 432, (×) 127, (△) 53, (○) 24.

crack tip region undergoes a little plastic deformation, but the triaxial stress achieves a larger level, the damage is similar to that in the SSY mode. With increasing deformation, the crack develops into a notch, the triaxial stress decreases; the damage is smaller than that in the SSY mode. The other important result, in the present context, is that the porosity converges to a configuration dependent porosity level at small values of $L\sigma_0/J$ with the increasing loads.

2.3.2. Crack tip openings

The crack tip opening displacement, δ_t, provides a convenient length scale to describe the deformation in the near tip region. Shih [36] defined δ_t as the separation where $\pm 45°$ lines emanating from the crack intercepts the opening faces, as shown in Fig. 5. The crack openings are calculated from SEN1, SEN2 and TPB specimens and the SSY mode, and are plotted against the loads of $J/\sigma_0 b_0$ in Fig. 6, where b_0 is the initial notch width, $b_0 = 2r_0$. It is observed that the crack opening in the SSY model is different from that in the actual specimens, i.e. the opening depends on the specimen's configuration. Therefore, to use the SSY mode in fracture analysis underestimates the crack tip opening.

2.4. Correlation of fracture toughness with SSY mode

In ductile fracture, where the dominant mechanism is void coalescence, the determination of fracture toughness, J_c, is related directly with the mechanism; mathematically, the criterion for void coalescence is assumed to be

$$f = f_{cr} \quad \text{at} \quad r = r_c \tag{22}$$

that is crack initiation occurs when the porosity exceeds a critical value over a characteristic distance, r_c, f_{cr} and r_c are the material's properties.

For a specific material, the void coalescence criterion is related to applied J values. From the damage distribution along the crack line shown in Fig. 4 for different specimens, it is found that in order to maintain an identical damage value at a characteristic position, r_c, for actual specimens and the SSY mode, larger applied load J values in the actual specimens need to be achieved. Based on the damage equivalence at the characteristic position in the SSY mode and actual specimens, the ratios of J_{SSY}: J, with damage values at a specific position may be obtained from damage distribution in Fig. 4, where J_{SSY} is refered to the J value in the SSY mode.

Since the fracture is not catastrophic, i.e. it involves some stable crack growth, the value r_c depends not only on the microstructure, but also on the method used to determine initiation of crack growth. In the presence of a precipitated second phase particle, initiation of a larger void is usual. Ritchie *et al.* [16] have reported the presence of precipitated carbide at the grain boundary, and hence the likely mode of failure

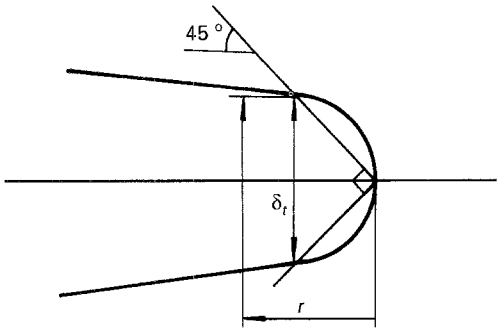

Figure 5 The 45° crack tip opening displacement [36].

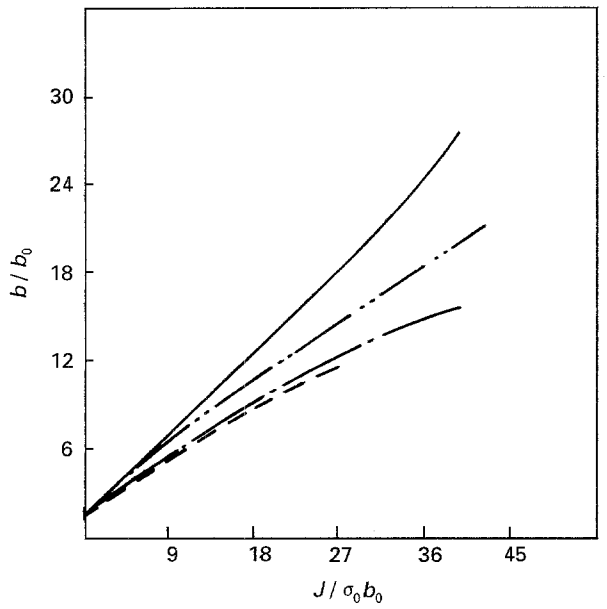

Figure 6 The crack openings, b/b_0, as a function of load, $J/\sigma_y b_0$, in (—·—) SEN1, (——) SEN2, (– – –) TPB specimens and (–) SSY mode.

involved nucleation of large voids at these carbides and failure by growth and linkage with other large voids. This may be due to voids of a different size nucleating between other voids and between the crack tip and the voids. Hence, the value of r_c appreciated to this case seems to be on the order of grain diameter. But for ductile fracture, the results of Jagota *et al.* recommended the value of r_c to be 2.5 grain diameters [17], and this is larger than the characteristic distance in cleavage mode [16] for a mild steel. For HY80 steel, Knott found, experimentally, that initiation of crack growth occurs when coalescence between the crack and a void nucleated at a particle with diameter, $2R_0$, takes place, and the distance, r, between the crack tip and the void satisfies that r/R_0 is 68 [37]. Therefore, the distance, r, is taken to be the characteristic distance, r_c, in the present study. The crack tip is simulated as a notch with a radius, r_0, of 5 μm; here, it is assumed that the diameter of the precipitated particle is on the order of the notch diameter. So that, 3, 4.3, 5 and 5.9 μm are taken as the particle radii of R_0, respectively, (this corresponds to an r_c of 204, 300, 340 and 400 μm, respectively) to obtain the ratio of J values in SSY mode to actual specimens. For different r_c, the ratio of J values in SSY mode to actual

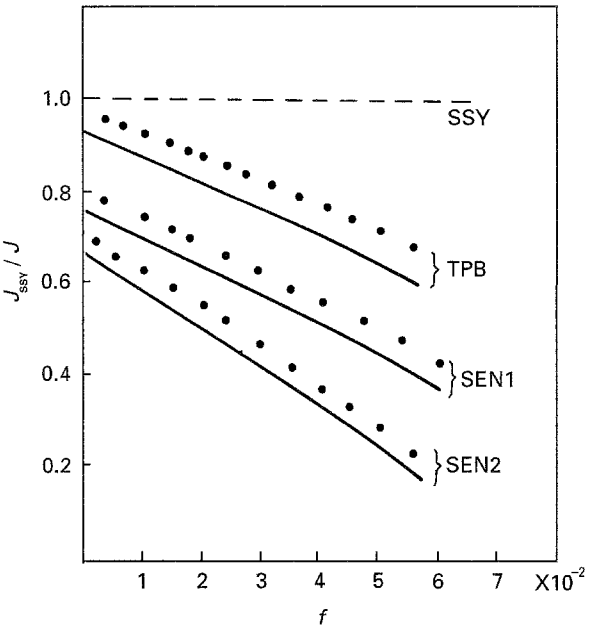

Figure 7 The ratios of J_{SSY} J values at: r_c equals (●) 204 and (—) 340 μm, respectively, with damage.

specimens at different damage values may be obtained. Fig. 7 shows that the ratios obtained for r_c are 204 and r_c 340 μm. It is clear that the ratios depend on the choice of the characteristic position of r_c; with increasing r_c values, the ratio J_{SSY}: J decreases, but the values of the ratios are always smaller than unity for r_c considered here.

To obtain the ratios of J values of different specimens at fracture initiation, the values of f_{cr} and f_c need to be determined first. Aravas and McMeeking have reviewed various coalescence criteria, these criteria were compared with finite element calculations of failure in ligament between the crack tip and a void using Gurson's model, the various criteria given were similar to those of LeRoy *et al.* [38], being closest to numerical calculations. According to these criteria, during void growth, shear localization occurs between neighbouring voids, leading to crack initiation. Coalescence is assumed to occur when the largest diameter of the void, d, is some fraction of the inter void spacing, D

$$d = kD \tag{23}$$

where d is the largest diameter of the void, k is a constant close to unity, and D is the intervoid distance. For spherical voids, k has been measured to have an average value of 0.83 for a number of steels, which coincides with the result observed by Hancock and Cowling [30] for HY80 steel. In the case of pores remaining roughly spherical ahead of the crack tip [23, 29], the pores are part of a simple cubic array, as shown in Fig. 8, and f may be expressed as [17]

$$f = \frac{\pi d^3}{6(d + D)^3} \tag{24}$$

using Equation 23, it is found

$$f_{cr} = 0.0489 \tag{25}$$

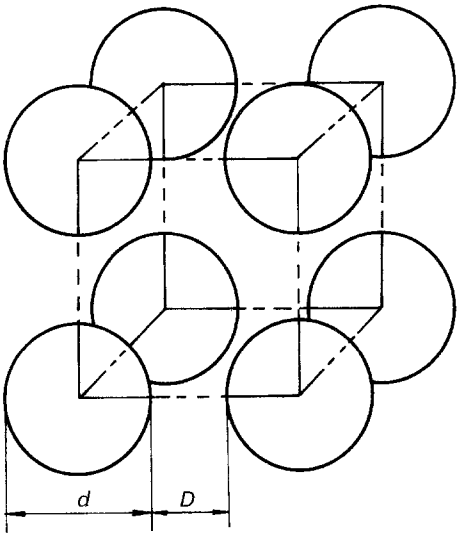

Figure 8 The geometry assumed in the derivation of f_{cr}, based on LeRoy void coalescence [38].

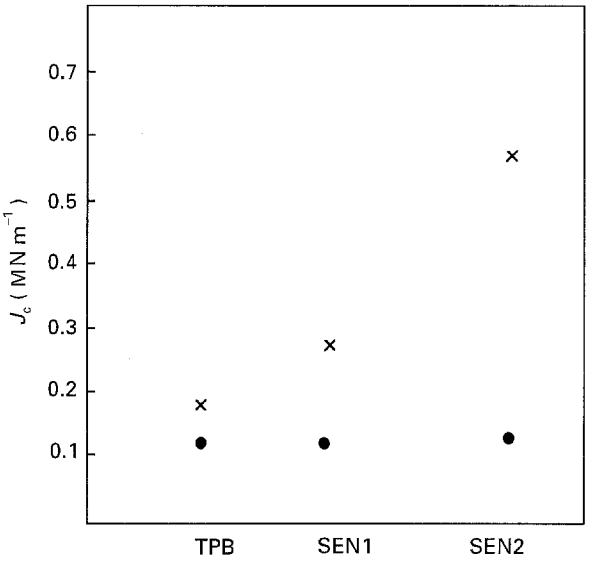

Figure 9 Experimentally (×) determined critical J values for different specimens [30] and corresponding (●) J_{SSY} values by damage equivalence at $r_c = 340$ μm.

This is close to the measured void fractions at fracture in LeRoy *et al.* [38].

Thus it is possible to obtain the ratio of J values in the actual specimen compared to that in the SSY mode (termed J_{SSY}) at fracture initiation from Equation 25 and Fig. 7. Using the ratio, the applications are two-fold

1. the geometry dependence of fracture toughness data can be eliminated through correlation to the SSY mode, and

2. commonly available test results for standard fracture specimens may be appreciably scaled for fracture assessments of non-standard notched structures. Hancock and Cowling have observed the initiation of crack growth in different specimens in HY80 steel, the crack openings in different specimens show obvious changes. According to the relation of J values and crack opening shown in Fig. 6, the critical J values in SEN1, SEN2 and TPB are given in Fig. 9, using the ratio of J: J_{SSY} shown in Fig. 7 and Equation 25, the critical J values are converted to J_{SSY} values, the J_{SSY} values for three of the specimens are shown in Fig. 9; it is found that the J_{SSY} values are almostly independent of specimen configuration.

3. Conclusions

The near crack tip porosity fields in different fracture specimens, single edge notched, single edge notched loaded in centre of ligament, three point bending specimens, and small scale yielding mode have been studied by the finite deformation finite element method. The presence and subsequent growth of smaller scale voids were taken into account by using Gurson's model to describe the constitutive behaviour of the material. For ductile fracture, where the dominant mechanism is void coalescence, the ratio of J values in the SSY mode to different specimens has been obtained numerically on the basis of damage equivalence at a characteristic position for both modes. The ratio of the J values is used to correlate the effects of geometry on fracture toughness.

Acknowledgements

This work was supported in part by the National Natural Science Foundation of China and Xian Jiaotong University. The author is also pleased to acknowledge helpful discussions with Professors Z. B. Kuang and T. J. Wang of Xian Jiaotong University.

References

1. J. R. RICE, *J. Appl. Mech.* **35** (1968) 379.
2. A. M. AL-ANI and J. W. HANCOCK, *J. Mech. Phys. Solids* **39** (1991) 23.
3. N. P. O'DOWD and C. F. SHIH, *ibid.* **39** (1991) 989.
4. *Idem., ibid.* **40** (1991) 939.
5. C. BETEGON and J. W. HANCOCK, *J. Appl. Mech.* **40** (1991) 104.
6. R. H. DODDS and C. F. SHIH, in "Proceedings of the IAEA/CSNI Specialists' Meeting on Fracture Mechanics Verification by Large Scale Testing", Tennessee, 26–29 October (1992).
7. Y. C. LI and T. C. WANG, *Scientia Sinica* **29A** (1986) 941.
8. M. F. ASHBY, in "Fracture Mechanics, Current Status, Future Prospects" (Pergamon Press, 1979) p. 1.
9. C. D. BEACHEM, *Trans. ASM.* **56** (1963) 318.
10. C. D. BEACHEM and G. R. YODER, *Metall. Trans.* **4** (1973) 1145.
11. K-H. SCHWALBE, *Engng. Fracture Mech.* **9** (1977) 795.
12. G. E. PELLISSIER, *ibid.* **1** (1968) 55.
13. G. GREEN and J. F. KNOTT, *J. Engng Mater. Technol.* **75** (1976) 37.
14. T. B. COX and J. R. LOW, *Metall. Trans.* **5** (1974) 1457.
15. S. H. GOODS and L. M. BROWN, *Acta Metall.* **27** (1979) 1.
16. R. O. RITCHIE, J. F. KNOTT and J. R. RICE, *J. Mech. Phys. Solids* **21** (1973) 395.
17. A. JAGOTA, C. H. HUI and P. R. DAWSON, *Int. J. Fracture* **33** (1987) 111.
18. R. H. DODDS, T. L. ANDERSON and M. T. KIRK, *ibid.* **48** (1991) 1.
19. T. L. ANDERSON and R. H. DODDS, *J. Test. Eval.* **19** (1991) 123.
20. J. R. RICE and M. A. JOHNSON, in "Inelastic Behaviour of Solids", edited by M. F. Kanninen, W. Adler, A. Rosenfield and R. Jaffee (McGraw-Hill, 1970) 641.

21. J. R. RICE and D. M. TRACEY, *J. Mech. Phys. Solids* **17** (1969) 201.
22. A. AOKI, K. KISHIMOTO, A. TAKEYA and M. SAKATA, *Int. J. Fracture* **24** (1984) 267.
23. N. ARAVAS and R. M. McMEEKING, *ibid.* **29** (1985) 21.
24. *Idem, J. Mech. Phys. Solids* **33** (1985) 25.
25. A. L. GURSON, *J. Engng Mater. Technol.* **77** (1977) 2.
26. V. TVERGAARD, *J. Mech. Phys. Solids* **30** (1982) 399.
27. V. TVERGAARD and A. NEEDLEMAN, *Acta Metall.* **32** (1984) 157.
28. A. NEEDLEMAN and V. TVERGAARD, *J. Mech. Phys. Solids* **35** (1987) 151.
29. F. MA and Z. B. KUANG, *Acta Metall. Mater.* **42** (1994) 497.
30. J. W. HANCOCK and COWLING, *Metal Sci.* **14** (1980) 293.
31. C. C. CHU and A. NEEDLEMAN, *J. Engng Mater. Technol.* **102** (1980) 249.
32. R. HILL "The Mathematical Theory of Plasticity" (Oxford University Press, 1950).
33. F. MA and Z-B. KUANG, in "Proceeding of the Joint FEFG/ICF", edited by S. H. Teoh and K. H. Lee (Singapore, 1991) p. 450.
34. Z. B. KUANG, *Engng Fracture Mech.* **19** (1984) 1161.
35. V. TVERGAARD, *Int. J. Solids Struct.* **18** (1982) 657.
36. C. F. SHIH, *J. Mech. Phys. Solids* **29** (1981) 305.
37. J. F. KNOTT, in "Conference Proceedings, Micromechanisms of Crack Extension", edited by J. F. Knott (1980).
38. G. LEROY, J. D. EMBURY, G. EDWARDS and M. F. ASHBY, *Acta Metall.* **29** (1981) 1509.

Received 15 February
and accepted 10 October 1994